

Article

# Optical Properties of Alkali Halides in Ultraviolet Spectral Regions

Khagendra P. Bhandari

Department of Physics and Astronomy, Ohio Northern University, Ada, OH 45810, USA; k-bhandari@onu.edu

Received: 22 May 2019; Accepted: 5 November 2019; Published: 11 December 2019



**Abstract:** The optical reflectance spectra of alkali halide crystals KI and RbI were measured over the energy range of 4.14 to 6.91 eV. Both single crystal and poly-crystal samples were used to accomplish this task. The phase  $\theta(\omega)$  was computed using the Kramers-Kronig relation between the real and imaginary parts of the complex function,  $\ln r = \ln |r| + i\theta(\omega)$ . Subsequently, the optical constants  $n$  and  $\kappa$  were determined from the Fresnel reflectivity equation. The real and imaginary parts of dielectric constants  $\epsilon_1$  and  $\epsilon_2$  were then calculated using  $n$  and  $\kappa$ . The optical absorption spectra of the crystal have also been measured in these spectral regions. The spectra agree reasonably well with the current theory concerning exciton peaks. In addition, a shoulder was found in the spectra similar to those previously seen and associated with the band-to-band transition in the alkali iodides.

**Keywords:** alkali halides; reflectance; absorption; optical constants; Kramers-Kronig

## 1. Introduction

The alkali halides KI and RbI crystallize in the NaCl structure under ambient conditions. The lengths of the sides of the unit cells for KI and RbI are 7.11 Å and 7.36 Å, respectively [1]. The electronic band structure of ionic crystals KI and RbI at room temperature suggests that insulator–metal transitions occur due to the reordering of the energy band where the empty, d-like band drops in energy below the top of the filled p-like bands [1]. The upper valence band located at the low energy part of the spectrum arises from the highest filled p states of the halogen ion [2,3]. The conduction band (the lowest  $\Gamma$  and X points) is mainly characterized by the positive ions in the lattice, as modeled by Onodera et al. [3] and Oyama et al. [4]. The experimental band gaps are 6.2 eV for KI and 6.1 eV for RbI [5]. The band structures of ionic solids suggest that they are direct band gap insulators at normal pressure [6,7]. The pressure dependence of the band gap suggests that KI and RbI are conventional ionic insulators whose band gaps decrease with increases in pressure [6].

Because of their simple crystal structures and bonding schemes, alkali halides have played a very important role in the development of solid-state physics. Their stability and availability in the form of single crystals of meaningful size, as well as of poly-crystals, have made them the subject of numerous experimental investigations. Physicists and material scientists have used alkali halides for testing their theories for several decades. The alkali halides were used to develop Debye’s theory of specific heat [8,9], Gruneisen’s theory of thermal expansion [10,11], Born’s theory of cohesions [12,13], Kellermann’s lattice dynamics [14,15], Lowdin’s very first application of quantum mechanics to crystal elasticity [16,17], and substrates for epitaxial growth studies in surface science [18–20]. More specifically, alkali iodides KI and RbI are of great physical interest, as they find application in the manufacture of opto-electronic devices and serve as typical models for other ionic compounds [21].

The fundamental optical properties of alkali halides have been extensively studied since 1930, when absorption measurements of the alkali halides were first carried out by Hilsch and Pohl [22]. However, it appears that there is still much to be learned from experiments done on these materials. In the early days, the optical properties of alkali halides were mostly studied for single crystals, and

were limited in terms of reflectivity studies and band structures. Before 1970, Baldini et al. studied the reflectivity data of many single-crystal alkali halides such as KI, KCl, KBr, RbI, RbCl, and RbBr in 5 eV to 10 eV [23,24]. Similarly, single-crystal alkali halides CsI [25], KI [26–29], KBr [30], and KCl [31] were also studied to calculate their optical constants. In contrast, studies of thin films of many alkali halides in the UV spectral region were limited in absorption measurements [32–34]. In addition, a literature review reveals a few more analyses of alkali halide crystals, such as a study on the influence of surface condition [35], on the strain effects on fundamental absorption [36], and on the effect of the layer thickness or uniaxial stress on the shape/location of exciton bands in RbI [37,38]. The literature on alkali halides has demonstrated that studies on the optical properties of RbI are comparatively limited. Cardona and Lynch studied the optical properties of a thin film of RbI, but their work was concentrated in the extreme ultraviolet region, i.e., from 50 eV to 250 eV [39]. S. Hashimoto and N. Momi-ie studied the interference effect and dispersion in thin RbI crystals [40]. The authors calculated the refractive indices in the spectral range of 4.8 eV to 5.7 eV, which is only part of the spectral range of present study. Similarly, the dielectric properties of single crystal RbI were discussed by Peimann and Skibowski in photon energies between 10 to 30 eV [41]. Finally, Roessler and Walker undertook research which was very similar to the present work for both KI and RbI single crystals [42]. They measured reflectance spectra in the range of 4–11 eV at 300 K and 77 K, respectively. Even though their first exciton peak matched with the present work for single crystal KI, the reflectance spectra for polycrystalline thin films of KI and RbI were not provided. Also, the authors used reflectance data measured at 77 K to calculate the real and imaginary parts of dielectric constants, instead of data measured at room temperature. They also did not calculate the refractive indices and absorption coefficient of the materials. The optical constants ( $n$  and  $\kappa$ ) and dielectric constants ( $\epsilon_1$  and  $\epsilon_2$ ) of a single crystal and poly-crystal thin film of RbI are subjects of interest for the scientific community, as these studies are lacking in the short- and medium-UV region.

In this work, the author presents the results of reflectance and transmittance measurements on single crystal and poly-crystal KI and RbI over a photon energy range of 300 nm (4.14 eV) to 180 nm (6.91 eV). From the reflectivity measurement, the wavelength-dependent refractive indices  $n(\omega)$  and  $k(\omega)$ , as well as dielectric constants  $\epsilon_1(\omega)$  and  $\epsilon_2(\omega)$ , are measured using Kramers-Kronig relations [43–45]. The behavior of the dielectric constants in any region of the spectrum can be analyzed according to the theories for various optical excitations of the crystal, such as the formation of electron-hole pairs commonly referred to as Excitons. Excitons form at the band gap energy of materials; thus, they are exceedingly important in studies of the electronic properties of photo conductors, and in the location of critical point energies in tertiary epitaxial materials such as AlGaAs [46].

## 2. Apparatus

A schematic of the experimental arrangement is shown in Figure 1. A high-pressure deuterium lamp served as a light source that provides a continuum of photon energies from 180–300 nm. The light was passed through a Czerny-Turner Monochromator with a grating of 2400 grooves/mm and suitable for wavelength range of 105 nm to 500 nm (Cornerstone 130, model: 77217). A highly-regulated power supply was connected in series with a (ELOGAR) C line conditioner that kept the intensity level steady to within 1% over the duration of the measurement. This was checked by examining the intensity of the source after the run in the 280 nm region, where RbI is transparent. The monochromator was driven by a stepping motor that allowed us to control the scanning rate and the dwell time at each step. The light output was observed using a 13-stage photomultiplier (Hamamatsu: R9875U) whose gain was flat in our region of interest. The photomultiplier tube detected radiation in the spectral range of 165 to 320 nm.

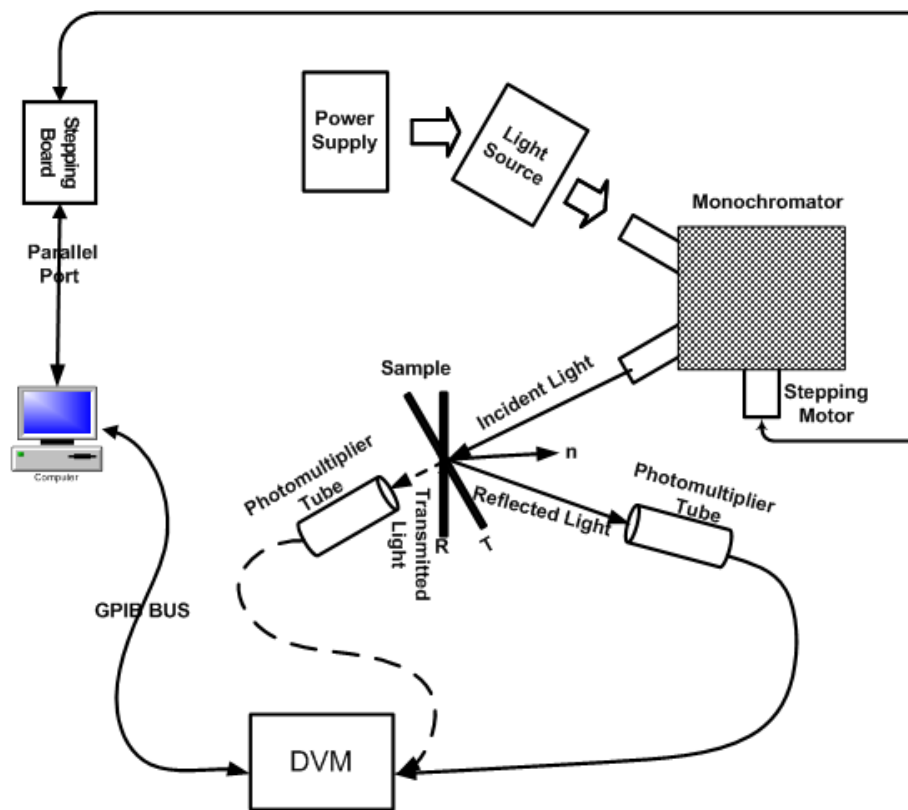


Figure 1. Schematic diagram of the instruments used.

Since the author worked in the non-visible energy range, it was important to ensure that the samples could be mounted and dismantled, keeping the geometry and optical alignment intact from one sample to another.

Samples were deposited from vapor at  $10^{-6}$  Torr. The substrates were Suprasil and Sapphire, both of which are transparent in the wavelength range of 170 nm to 5.3  $\mu\text{m}$ . Suprasil is a high quality synthetic fused silica material (amorphous grade of silica) manufactured by flame hydrolysis of  $\text{SiCl}_4$ . Sapphire is the single crystal form of aluminum oxide ( $\text{Al}_2\text{O}_3$ ). The use of these two different materials ensured that all the measurements were independent of the substrate and substrate interface to some extent.

### 3. Experimental Methods

The substrate and tantalum evaporation boats were cleaned using particle-free water, followed by methanol, and dried with dry nitrogen gas. The boats were then heated in a vacuum to 300  $^\circ\text{C}$  for several minutes to drive off impurities. Subsequently, the boats were loaded with 0.9999-purity RbI chips (or with KI), and the substrates were mounted in the vacuum for evaporation. The system was evacuated overnight before growing the sample. The samples were grown at a pressure of  $\sim 1 \times 10^{-6}$  Torr, when the evaporation rate was in the range of 0.2 nm/s to 0.4 nm/s.

Since RbI and KI are hygroscopic, the grown sample was kept in a dry nitrogen atmosphere until it was transferred to the experimental setup. Before the sample was taken out, it was covered with another suprasil (or sapphire) glass blank to prevent it from being contaminated by atmosphere. The sample was covered only for the lengthy transmission measurements (more data were taken in transmittance measurements than reflectance measurements, even in the same spectral range, to improve the quality of data.).

For reflectance, single crystal samples grown commercially were also used. To measure reflectivity, the intensity of the reflected light from the sample and the intensity of the incident beams were measured. Then, the reflectivity ( $R$ ) was calculated by taking the ratio of the reflected and incident

light. The intensities of the transmitted light from the single crystals could not be measured, as they were too thick, and the transmitted light was below the noise level.

For the measurement of the film thickness, the masses of the substrate before and after growing the crystal were measured; the difference between the two masses was the mass of the crystal grown. Then, the diameter of the circular substrate was measured, and the cross-sectional area was calculated. Using the mass and density obtained from the handbook of Chemistry and Physics [47], the thicknesses of the films were calculated by dividing the volume by the cross-sectional area. The thicknesses of the KI and RbI films were  $\sim 1.039 \pm 0.177 \mu\text{m}$  and  $\sim 0.916 \pm 0.156 \mu\text{m}$ , respectively.

#### 4. Theory

To describe the response of a medium to electromagnetic fields as a function of space and time, we can use either the complex dielectric function  $\tilde{\epsilon}(\omega)$ , consisting of real and imaginary dielectric constants ( $\epsilon_1, \epsilon_2$ ), or the complex index of refraction  $\tilde{n}(\omega)$ , consisting of the real and imaginary index of refractions ( $n, \kappa$ ). The complex index of refraction is related to dielectric constants by [48]

$$\tilde{n}^2 = \epsilon_1 + i\epsilon_2 \quad (1)$$

Optical constants  $n$  and  $\kappa$  are also defined by writing out the complex index of refraction  $\tilde{n}$  as

$$\tilde{n} = n(\omega) + i\kappa(\omega) \quad (2)$$

The imaginary index of refraction,  $\kappa$ , also known as the extinction coefficient, measures the attenuation of the wave in the medium. When losses are absent,  $n$ , which plays the role of an index of refraction, is just the ratio of the velocity of light in empty space to the velocity in the medium.

Squaring both sides of (2) and comparing with (1), we get

$$\begin{aligned} \epsilon_1(\omega) &= n^2(\omega) - \kappa^2(\omega) \\ \epsilon_2(\omega) &= 2n\kappa \end{aligned} \quad (3)$$

In the case of normal incidence, the complex reflection coefficient (also called Fresnel reflection coefficient) is given by [49]

$$\tilde{r} = \frac{E_r}{E_i} = \frac{n - 1 + i\kappa}{n + 1 + i\kappa} = \frac{\tilde{n} - 1}{\tilde{n} + 1} \quad (4)$$

It is sometimes convenient to write  $\tilde{r}$  in terms of an amplitude  $|r|$  and a phase shift upon reflection  $\theta$ , that is

$$\tilde{r} = |r|e^{i\theta(\omega)} = |r|(\cos \theta(\omega) + i \sin \theta(\omega)) \quad (5)$$

Experimentally, we do not measure  $\tilde{r}$ , but we do measure the reflection coefficient  $R(\omega)$ :

$$R(\omega) = |r|^2 = \frac{(n - 1)^2 + \kappa^2}{(n + 1)^2 + \kappa^2} \quad (6)$$

It is difficult to measure the phase angle  $\theta(\omega)$  of the reflected wave, but it can be calculated from the measured reflectance  $R(\omega)$  if we know it for all frequencies [50]. The phase change  $\theta(\omega_0)$  at a particular frequency,  $\omega_0$ , between the incidence and the reflected signal is obtained from the Kramers-Kronig dispersion relation [51]:

$$\theta(\omega_0) = -\frac{\omega_0}{\pi} P \int_0^\infty \frac{\ln R(\omega) d\omega}{\omega^2 - \omega_0^2} \quad (7)$$

where  $P$  stands for the Cauchy principle value of the integral; singularity in the integral at  $\omega = \omega_0$  is omitted from the integration. Simplifying (7) by integrating by parts gives insight into the contribution to the phase angle  $\theta(\omega_0)$  as

$$\theta(\omega_0) = \frac{1}{2\pi} \int_0^\infty \frac{d \ln R(\omega)}{d\omega} \ln \left| \frac{\omega + \omega_0}{\omega - \omega_0} \right| d\omega, \quad (8)$$

The logarithmic weighting function in (8) becomes small for frequencies far from  $\omega_0$ . Thus, it reduces the relative contribution to the integral at such frequencies. Also,  $\ln R(\omega)$  appears as a derivative in the integrand, so there is no contribution to the integral for the frequencies where the reflectance is constant, and positive and negative slopes on the same side of  $\omega_0$  tend to cancel each other out. The phase in radians at  $\omega_0$  is thus obtained from Equation (8) by numerical integration using a computer.

Having determined a value of  $\theta(\omega_0)$  for a given frequency, the real and imaginary parts of the complex refractive index  $\tilde{n} = n + i\kappa$  are obtained using Equations (4) and (5) as following.

$$\frac{n+i\kappa-1}{n+i\kappa+1} = |r|(\cos \theta(\omega) + i \sin \theta(\omega))$$

Now, simplifying the above expression the real and imaginary parts of refractive indices can be calculated as

$$n = \frac{1 - |r|^2}{1 + |r|^2 - 2|r| \cos \theta(\omega)} \quad (9)$$

$$\kappa = \frac{(n + 1)|r| \sin \theta(\omega)}{|r| \cos \theta(\omega) - 1} \quad (10)$$

The real and imaginary parts of the complex dielectric constants are then determined using Equation (3), and absorption coefficient  $\alpha$  by the relation

$$\alpha = \frac{4\pi\kappa}{\lambda} \quad (11)$$

## 5. Results and Discussion

For a comparison with past work, we present some results for KI [26,32,52]. The absolute reflectance of KI was measured from one polished single crystal and one poly-crystal grown in a vacuum system for photon energies ranging from 4.14 to 6.91 eV. The spectra of reflectance from a thick single crystal and a thin poly-crystal are shown in Figure 2a,b, respectively. In Figure 2a, we have compared present work (solid line) with previous work (dashed line) by H. R. Philipp et al. [26]. The prominent peaks in these spectra are at photon energies 5.62 eV for the thick and 5.64 eV for the thin sample, respectively. Proceeding to the lower energies in Figure 2a,b, the structure to be noted is at photon energy 5.18 eV for the thick and 5.17 eV for the thin sample, respectively. Similarly, proceeding to the higher energies, the next structures to be noted are the shoulders at  $h\omega = 6.08$  eV for the thick and 6.03 eV for the thin sample. The next prominent peaks in the reflectance are observed at  $h\omega = 6.68$  and 6.64 eV in both cases.

Since excitons in alkali halides are localized on an atomic level, the results for single crystals and poly-crystals are very similar, and appear to be in agreement with the results of previous investigators. We next considered RbI where some results are unknown.

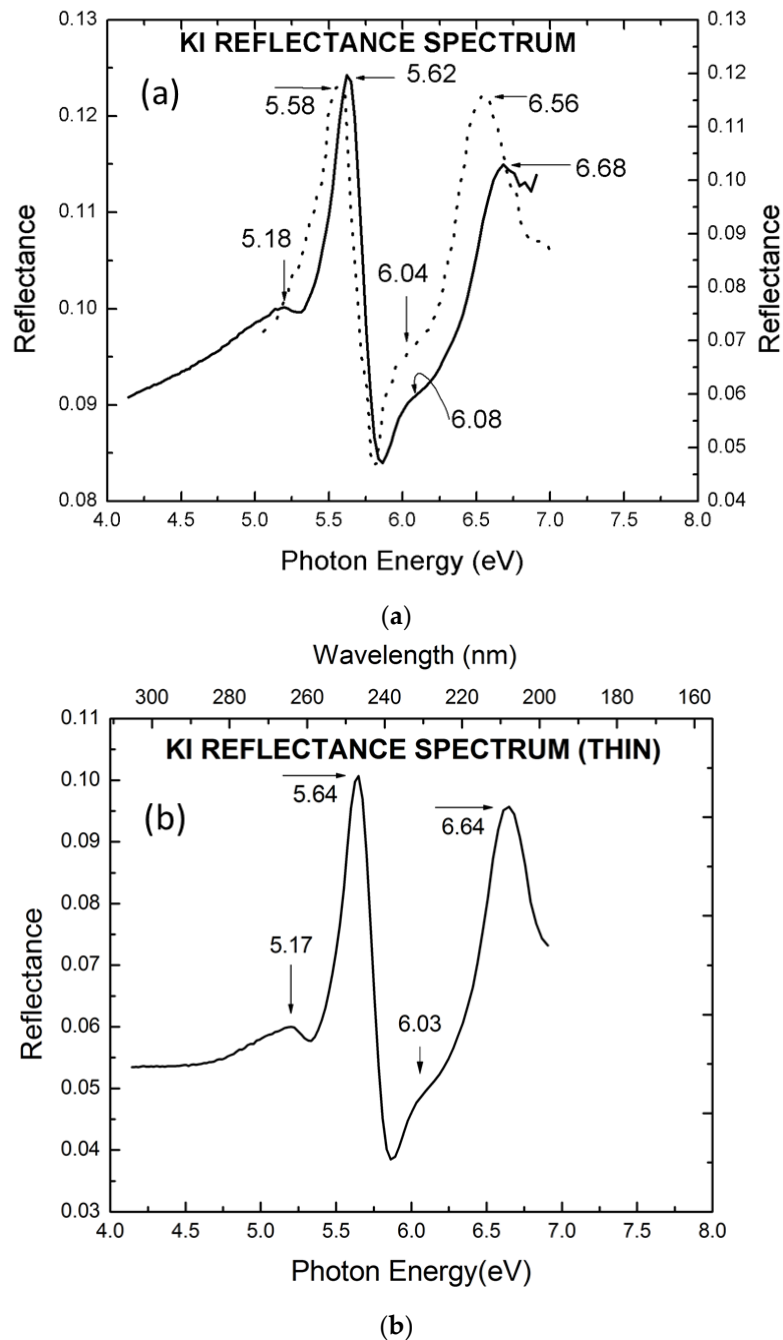


**Figure 2.** (a) Spectral dependence of the reflectance of KI (Single crystal). The result for a reflectance spectrum by H. R. Philipp et al. [26] is shown by the dashed curve; (b) Spectral dependence of the reflectance of KI (poly-crystal).

The spectrum for reflectance of RbI is shown in Figure 3. The prominent reflectance peaks are indicated by arrows. RbI and KI have the same lattice structure, comparable lattice constants, ionic bonds, and noble gas configurations that exhibit tightly-bound excitons [53,54]. Thus, the absorption and reflectance spectra for RbI and KI should exhibit similar features.

According to Equation (2), in the theory section, the refractive index is defined to be complex. The real part ( $n$ ) relates to the velocity of light in the medium for a given frequency, and imaginary part ( $\kappa$ ) relates to the attenuation of amplitude of the wave due to absorption. In the case of normal incidence, the Fresnel reflection coefficient is given by Equation (4), and reflectance is measured by Equation (6). From Equation (6), it is clear that for strong reflectivity, both  $n$  and  $\kappa$  must be larger. At photon energies

above the band gap, strong absorption contributes considerably to reflectivity. It is clear from Figure 4 that  $n$  and  $\kappa$  are larger for single crystalline materials, providing larger reflectivity, as in Figures 2 and 3.

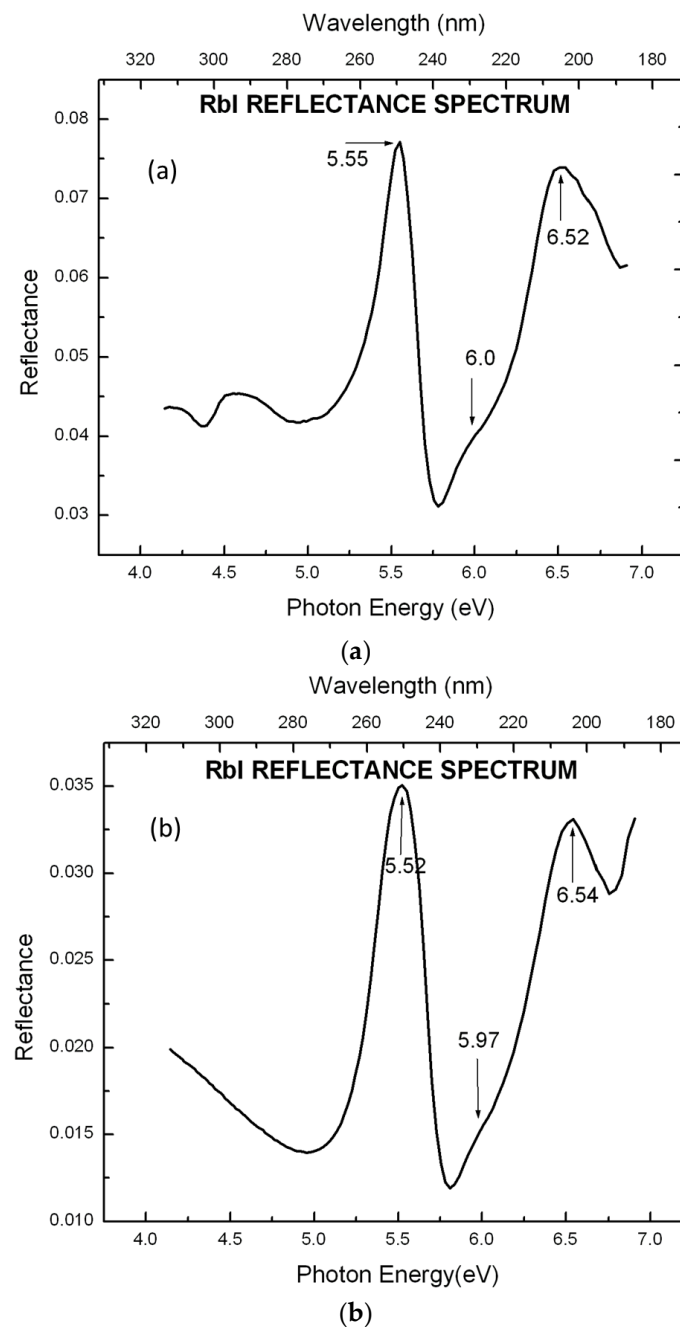


**Figure 3.** Reflectance spectrum of RbI (a) thick sample; (b) thin sample. The prominent peaks in both cases are shown by arrows with magnitudes.

Reflection from the surface of a material is a combination of both diffuse and specular reflection components. As poly-crystalline materials are made up of many smaller crystallites with varying orientations, reflection from them is just like a diffuse reflection. In specular reflections, the angle of reflection is equal to the angle of incidence, and occurs when the incident light is reflected from a smooth surface such as the film of single crystalline materials. When the film fabrication is complete, sometimes the formation of defect states is unavoidable; these states act as scattering centers for the beam of incident light, causing diffuse reflection. Similarly, grain boundaries are the sources of scattering centers in poly-crystalline thin films. Single crystalline materials with no or negligible defect

states and with no grain boundaries keep the reflectivity higher than polycrystalline materials, as shown in Figures 2 and 3. Reflectivity also depends on other factors such as the angle of incidence and the polarization of the radiation.

The optical constants of RbI are presented in Figure 4. Figure 4a gives the real ( $n$ ) and imaginary ( $\kappa$ ) parts of the complex refractive index ( $\tilde{n} = n + i\kappa$ ) for the thick sample, and Figure 4b gives the corresponding values for thin samples. Figure 4c,d depict the real ( $\varepsilon_1$ ) and imaginary ( $\varepsilon_2$ ) parts of the complex dielectric constants ( $\tilde{\varepsilon} = \varepsilon_1 + i\varepsilon_2$ ) for the thick and thin samples respectively.

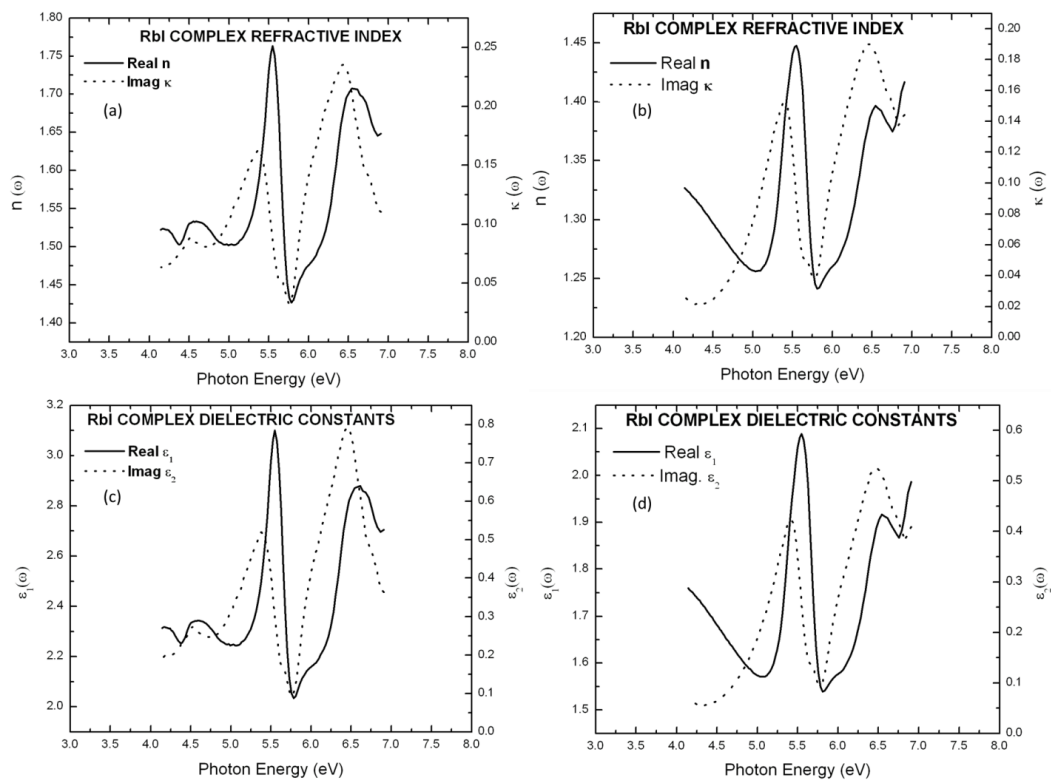


**Figure 4.** Real and imaginary parts of the RbI refractive index: (a) thick sample (b) thin sample as determined from the reflectance spectrum; Real and imaginary parts of the RbI complex dielectric constants: (c) thick sample (d) thin sample as determined from the reflectance spectrum.

The RbI optical absorption coefficient is presented in Figure 5. The photon energies at which the structures appear are marked with arrows. The positions of the structures, however, are somewhat different from those of the reflectance spectrum of Figure 2. The prominent peaks of the optical absorption coefficients are very large in magnitude; some are in excess of  $\alpha \approx 10^5 \text{ cm}^{-1}$ . Therefore, the film thickness has to be a micron or less for conventional transmission measurements to be performed. The prominent peaks for absorption (5.4 eV, 6.01 eV, and 6.46 eV) are at slightly different photon energies than the experimental peaks that are given by optical density (5.64 eV, 6.02 eV, and 6.53 eV) of the thin films. This could be attributed to the fact that approximations made in applying Kramers-Kronig relations to the reflectance spectrum are not truly valid.

As in Equation (8), the phase shift on reflection of radiation of frequency  $\omega_0$  is supposed to be calculated for the entire range  $0 \leq \omega_0 \leq \infty$ . However, the experimental data can never be available for the entire range  $0 \leq \omega_0 \leq \infty$ . The usual approach to minimize the error in the calculation has been to measure the data over as wide range as possible, and if necessary, to extrapolate the data on both sides of the experimental range as reasonably as possible into a region where it ceases to influence the integration. Even without doing this, the calculated data are very close to the experimental data, as shown in Figures 5b and 6b.

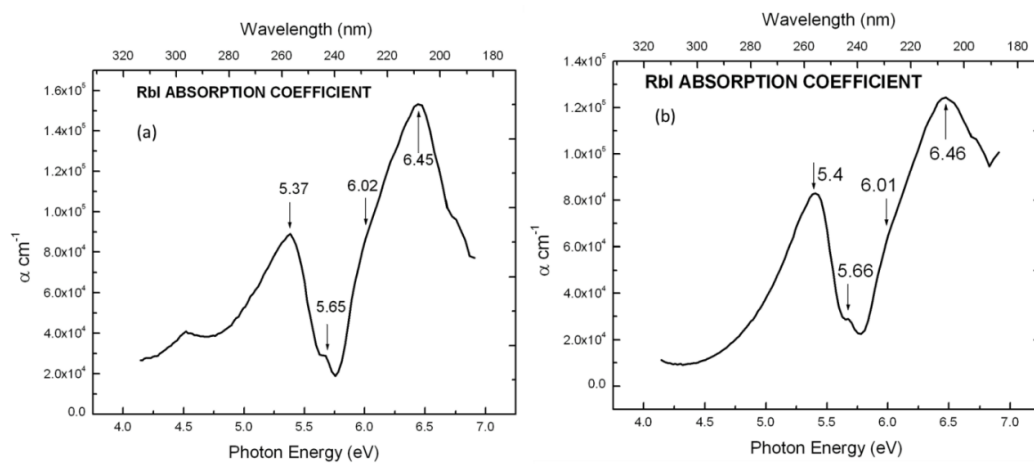


**Figure 5.** Optical-absorption coefficients of RbI (a) thick sample and (b) thin sample. The prominent peaks are indicated by arrows with magnitudes.

As  $n$  and  $\kappa$  are frequency dependent, their values even for the same crystal are different for different frequencies. Tables 1 and 2 summarize the results of refractive index  $n$  for single and poly-crystalline samples.

**Table 1.** Refractive Index ( $n$ ): Thick Single Crystal Sample.

Materials	Maximum	Minimum
KI	2.04 (5.63 eV)	1.55 (5.86 eV)
RbI	1.76 (5.63 eV)	1.43 (5.78 eV)

**Table 2.** Refractive Index ( $n$ ): Thin Poly-crystal Sample.

Materials	Maximum	Minimum
KI	1.93 (5.65 eV)	1.49 (5.86 eV)
RbI	1.45 (5.55 eV)	1.24 (5.81 eV)

Dielectric function describes the response of the crystals to an electromagnetic field. When an electromagnetic wave is incident on the crystal, it gets polarized. The polarization is due to the motion of the valence electrons (electronic polarization) as well as displacements of the crystal ions (lattice polarization). The relative effects of these two polarizations contribute to the dielectric functions. Similar to refractive index, we have summarized the results of the real part of dielectric constants in Tables 3 and 4 respectively.

**Table 3.** Dielectric constants (real parts): Thick Single Crystal Sample.

Materials	Maximum	Minimum
KI	4.14 (5.63 eV)	2.40 (5.86 eV)
RbI	3.10 (5.55 eV)	2.03 (5.78 eV)

**Table 4.** Dielectric constants (real parts): Thin Poly-crystal Sample.

Materials	Maximum	Minimum
KI	3.71 (5.65 eV)	2.21 (5.86 eV)
RbI	2.09 (5.55 eV)	1.54 (5.81 eV)

The real parts of the dielectric constants and refractive indices are similar to the reflectance spectrum, and the imaginary parts are also somewhat similar to the optical density of the crystals,

as expected. The data presented in Tables 3 and 4 support the fact that alkali halides are associated with their relatively small dielectric constants. Such a small dielectric constant makes the Coulomb interaction  $-\frac{e^2}{\epsilon(r)r^2}$  between the electrons and holes correspondingly strong.

The optical density of KI and RbI have been calculated from the intensity of transmitted light as measured from the thin samples. Graphs of optical densities with respect to photon energy are presented in Figure 6. Also, the work of J. E. Eby et al. [32] can be seen (dashed line). The structures are marked with arrows.

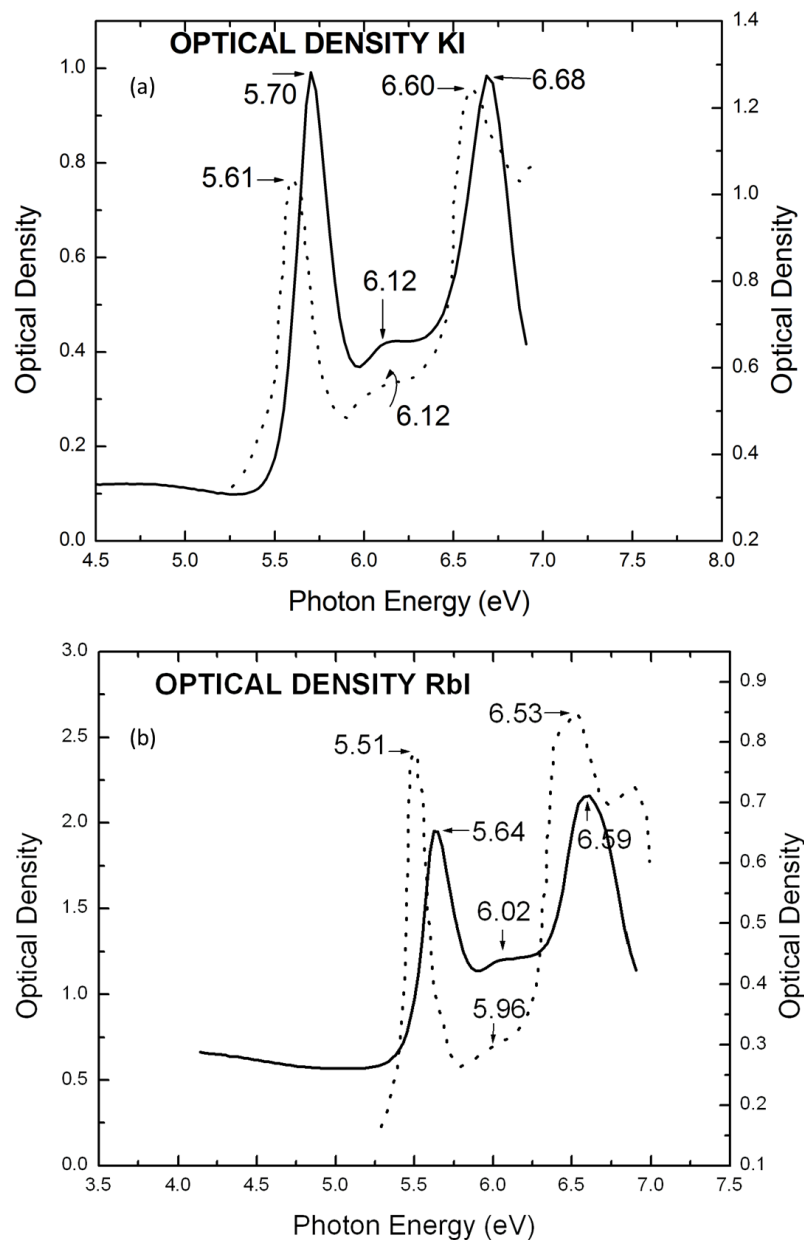


**Figure 6.** (a) Optical absorption spectra of thin films of the KI deposited on suprasil substrate, solid line, in comparison with measurements by J. E. Eby et al. [32], shown by the dashed line, where the KI was deposited on LiF. The results are for room temperature. (b) The optical absorption spectra of thin films of RbI deposited on sapphire substrate. The measurements were done at room temperature for RbI. The result of the optical absorption spectra by J. E. Eby et al. [32] is shown by the dashed line. The film of RbI was deposited on LiF.

The small energy shift between the present results and Eby's could not be accounted for, except for the difference between the amorphous and crystalline substrates. Temperature difference could not account for the fact that peaks in Eby's data occur at lower energy. Similarly, the narrowness of the peaks in both cases suggests that both samples were pure and crystalline. Thus, we can only conclude that the substrate/interface affects exciton energy and is responsible for the shift to the lower energy observed in Eby's data. Lattice matching is essential to grow high quality thin films. In case there is slight mismatch between the substrate and the film, there is some strain on the films, which probably affects some of the properties of the overgrown layer on the substrate. Besides lattice matching, the thermal and chemical stability and thermal expansion coefficients of the substrate can also influence the properties of deposited films. If there are similarities in the lattices between the film and the substrate, then the promotion of epitaxial growth is possible with the same or different crystal structures.

In the present work, sapphire and suprasil are used as substrates, where suprasil is amorphous in nature, but sapphire ( $\text{Al}_2\text{O}_3$ ) has hexagonal crystal structure ( $a = 4.785 \text{ \AA}$ ,  $c = 12.991 \text{ \AA}$ ). In a work by Eby et al. [32], LiF was used as a substrate which has a cubic crystal structure ( $a = 4.02 \text{ \AA}$ ) similar to that of KI and RbI ( $a_{\text{KI}} = 7.06 \text{ \AA}$  and  $a_{\text{RbI}} = 7.342 \text{ \AA}$ ). Therefore, small differences in peak position between the present data and Eby's data may appear from substrate/interface effects. Although impurities can shift the band edge to the lower energy, impurities would also broaden the exciton peaks [33].

A direct interband threshold has been identified as a shoulder in the absorption spectrum. The shoulders in KI and RbI fall at 6.12 and 6.02 eV, respectively, as shown in Figure 6. The positions of the shoulders in KI and RbI agree fairly well with those found in the absorption spectra by K. Teegarden et al. [33]. They have found these shoulders to be located at 6.2 and 6.1 eV at 10 K. The appearance of these shoulders was also found to be the same as those previously reported and discussed by Taft and Phillip and others [32,52]. The band gap energy increases as the temperature is decreased.

Band structure calculations for the ionic crystals show that the valence bands, originating from the filled p states of the negative ions (halogen ions), are about 0.75 eV wide [2–4,55–58]. The corresponding wave functions are localized on the negative halogen ions sites, and have a strong p character [55,58]. The important structure in the valence band is determined by the spin-orbit splitting parameter  $\eta$ . The splitting parameter can be estimated [32] from the splitting of the free halogen doublet by  $\frac{3\eta}{2}$ . This gives the separation of the ground state doublet of the free halogen atom. For iodine, the value of  $\eta$  is 0.63 eV. Similarly,  $\eta$  for chlorides is about 0.1 eV, and for bromides 0.4 eV. For KI, the first peak of the doublet is at 5.70 and the second at 6.68 eV, i.e., split by 0.98, as expected from the iodine splitting of 0.945 eV (calculated from  $\frac{3\eta}{2}$ ). Similarly, in the RbI spectrum shown in Figure 6, the doublet is at 5.64 eV and 6.59 eV, a split of 0.95 eV, compared with the expected 0.945 eV. The values of these peaks, as determined by J. C. Phillips [5], are shown in Table 5.

**Table 5.** Splitting of the halogen doublets at 80K [32].

Materials	First Peak	Second Peak	Difference
KI	5.80 eV	6.68 eV	0.88 eV
RbI	5.70 eV	6.47 eV	0.77 eV
NaI	5.56 eV	6.73 eV	1.17 eV
CsI	5.76 eV	5.91 eV	0.15 eV
LiI	uncertain	uncertain	

The optical densities of KI and RbI (present work) were compared with those of NaI, CsI, and LiI taken from Eby et al. [32], as shown in Figure 7. All spectra are compared in the same spectral energy range except for LiI, where absorbance spectra are provided only from 6.4 eV to higher energy, due to its comparatively high energy band gap  $\sim 6.6 \text{ eV}$  [59]. Thin films of NaI, CsI, and LiI were grown on a LiF substrate, and spin orbit splitting of the halogen doublet for each alkali halide was calculated at 80 K. The splitting of halogen doublets is provided in Table 5. The splitting of CsI and NaI was inconsistent with the expected values, whereas this value for LiI could not be determined.

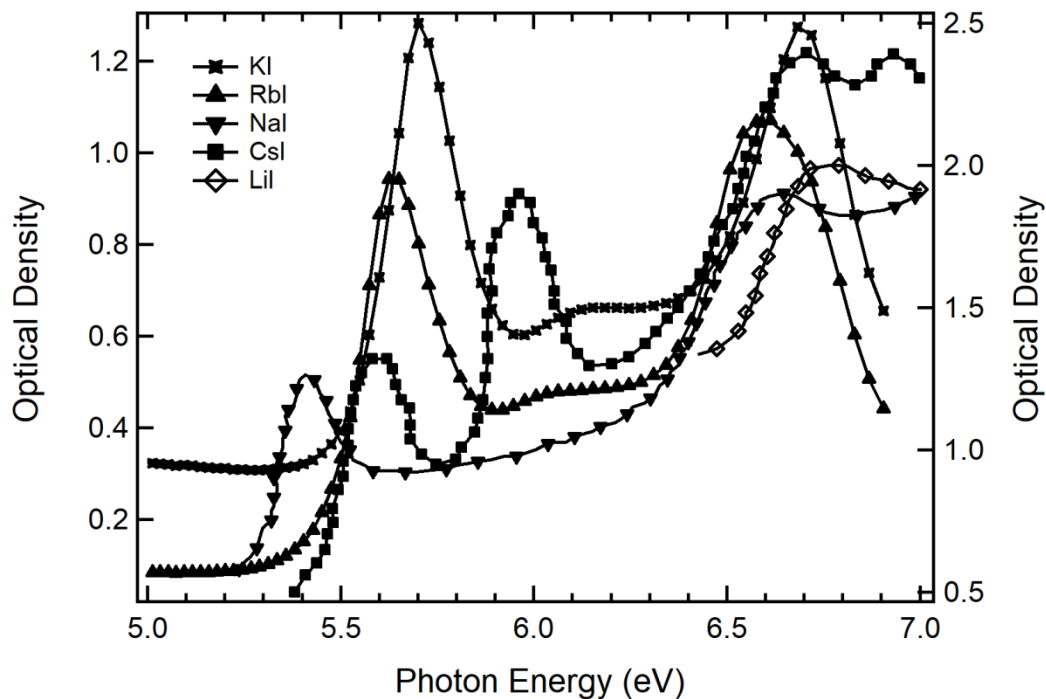


**Figure 7.** Optical absorption spectra of thin films of different alkali halides; spectra for KI and RbI are from the present work (axis to the right), whereas spectra for NaI, CsI, and LiI are taken from from J. E. Eby et al. [32] (axis to the left). The measurements were made at room temperature for KI and RbI and at 80 K for the three other compounds.

## 6. Conclusions

The author presents normal incidence-reflectance spectra of KI and RbI in the ultraviolet spectral regions, and uses the Kramers-Kronig (KK) theory to analyze some of these spectra. The application of KK theory produced nearly the same results for both single and poly-crystalline samples of RbI. The author also demonstrates and analyzes absorbance spectra of KI and RbI, and finds that the present results are more accurate than previously published work, as is clear from the spin-orbit splitting parameters. The peaks observed in the reflectance or absorbance spectra of KI and RbI are caused by excitons associated with critical points (second derivative of  $\epsilon_1$  w.r.t. energy). Excitons are especially important in these insulators because of the electron-hole interaction in the absence of strong screening. Due to the small dielectric constant, Coulomb interactions between an electron and a hole are strong, and excitons thus tend to be small. Since the excitonic peaks are sharp and very well separated, the optical properties of alkali halides are localized on an atomic level. Finally, it may be concluded that the shift in the absorbance peak positions in energy found in this work in comparison with the results of J. E. Eby et al. [32] appears to be attributable to the substrate-sample interface. Impurities and substrate effects would generally occur at lower energy.

**Funding:** K. Bhandari received support from summer research grant, College of Arts and Sciences, Ohio Northern University.

**Acknowledgments:** The author greatly appreciates Michael Sydor, department of physics, the University of Minnesota, Duluth for helpful suggestion during the preparation of this manuscript.

**Conflicts of Interest:** The authors declare no conflicts of interest.

## References

1. Louis, C.N.; Iyakutti, K. Electronic band structure and metallization of KI and RbI under high pressure. *Phys. Status Solidi* **2002**, *233*, 339–350. [[CrossRef](#)]
2. Howland, L. Band structure and cohesive energy of potassium chloride. *Phys. Rev.* **1958**, *109*, 1927. [[CrossRef](#)]

3. Onodera, Y.; Okazaki, M.; Inui, T. Relativistic electronic structure of KI crystal. *J. Phys. Soc. Jpn.* **1966**, *21*, 2229–2238. [[CrossRef](#)]
4. Oyama, S.; Miyakawa, T. Conduction band structure of KCl. *J. Phys. Soc. Jpn.* **1966**, *21*, 868–874. [[CrossRef](#)]
5. Phillips, J. Ultraviolet absorption of insulators. III. fcc alkali halides. *Phys. Rev.* **1964**, *136*, A1705. [[CrossRef](#)]
6. Amirthakumari, R.M.; Pari, G.; Rita, R.; Asokamani, R. Phase transformation and metallisation studies of some of the alkali iodides through high pressure electronic structure calculations. *Phys. Status Solidi* **1997**, *199*, 157–164. [[CrossRef](#)]
7. Ching, W.; Gan, F.; Huang, M.Z. Band theory of linear and nonlinear susceptibilities of some binary ionic insulators. *Phys. Rev. B* **1995**, *52*, 1596. [[CrossRef](#)]
8. Ketterson, J.B. The Physics of Solids. *MRS Bull.* **2018**, *43*, 68–69.
9. Dayal, B. The specific heats of the alkali halides. *Proc. Indian Acad. Sci.Sect. A* **1944**, *20*, 77–86. [[CrossRef](#)]
10. Dayal, B. Theory of the thermal expansion of the alkali halides. *Proc. Indian Acad. Sci.Sect. A* **1944**, *20*, 145–154. [[CrossRef](#)]
11. White, G. The thermal expansion of alkali halides at low temperatures. *Proc. R. Soc. Lond. A* **1965**, *286*, 204–217.
12. Doll, K.; Stoll, H. Cohesive properties of alkali halides. *Phys. Rev. B* **1997**, *56*, 10121. [[CrossRef](#)]
13. Slater, J.C. Compressibility of the Alkali Halides. *Phys. Rev.* **1924**, *23*, 488–500. [[CrossRef](#)]
14. Basu, A.N.; Sengupta, S. Lattice Dynamics of Alkali Halides. *Phys. Rev. B* **1973**, *8*, 2982. [[CrossRef](#)]
15. Woods, A.; Cochran, W.; Brockhouse, B. Lattice dynamics of alkali halide crystals. *Phys. Rev.* **1960**, *119*, 980. [[CrossRef](#)]
16. Verma, M.; Dayal, B. Fuchs's Relations in Alkali Halides and Their Application to the Lattice Dynamics of Lithium Fluoride. *Phys. Status Solidi* **1966**, *13*, 251–256. [[CrossRef](#)]
17. Singh, R.; Verma, M. Effect of Three-Body Forces on the Shell Model of Alkali Halides: Application to KBr and KI. *Phys. Status Solidi* **1969**, *36*, 335–343. [[CrossRef](#)]
18. Jesser, W.A.; Matthews, J.W. Growth of copper, silver, and gold on twelve Alkali halides cleaved in vacuum. *J. Cryst. Growth* **1969**, *5*, 83–89. [[CrossRef](#)]
19. Lord, D.G.; Prutton, M. Electrons and the epitaxial growth of metals on alkali halides. *Thin Solid Films* **1974**, *21*, 341–356. [[CrossRef](#)]
20. Mobus, M.; Karl, N.; Kobayashi, T. Structure of perylene-tetracarboxylic-dianhydride thin films on alkali halide crystal substrates. *J. Cryst. Growth* **1992**, *116*, 495–504. [[CrossRef](#)]
21. Gupta, S.C. *Optoelectronic Devices and Systems*; PHI Learning Pvt. Ltd.: Delhi, India, 2014.
22. Hilsch, R.; Pohl, R.W. Einige Dispersionsfrequenzen der Alkalihalogenidkristalle im Schumanngebiet. *Z. Phys.* **1930**, *59*, 812–819. [[CrossRef](#)]
23. Baldini, G.; Bosacchi, B. Optical properties of alkali-halide crystals. *Phys. Rev.* **1968**, *166*, 863. [[CrossRef](#)]
24. Baldini, G.; Bosacchi, A.; Bosacchi, B. Exciton-phonon interaction in alkali halides. *Phys. Rev. Lett.* **1969**, *23*, 846. [[CrossRef](#)]
25. Said, K.I.; Green, G.W. Optical properties of caesium iodide in the vacuum ultraviolet. *J. Phys. C* **1977**, *10*, 479–488. [[CrossRef](#)]
26. Philipp, H.R.; Ehrenreich, H. Intrinsic Optical Properties of Alkali Halides. *Phys. Rev.* **1963**, *131*, 2016. [[CrossRef](#)]
27. Blechschmidt, D.; Klucker, R.; Skibowski, M. Dielectric properties of KCl, KBr, and KI single crystals in the extreme ultraviolet up to 35 eV. *Phys. Status Solidi* **1969**, *36*, 625–634. [[CrossRef](#)]
28. Tomiki, T.; Miyata, T.; Tsukamoto, H. Temperature Dependence of the Fundamental Spectra of Potassium-Halides in the Schumann Ultraviolet Region (4.4~13.5 eV). *J. Phys. Soc. Jpn.* **1973**, *35*, 495–507.
29. Tomiki, T.; Miyata, T.; Tsukamoto, H. The Urbach rule for the sodium-and potassium-halides. *Z. Naturforsch. A* **1974**, *29*, 145–157. [[CrossRef](#)]
30. Antinori, M.; Balzarotti, A.; Piacentini, M. High-resolution reflection spectra of alkali halides in the far ultraviolet. *Phys. Rev. B* **1973**, *7*, 1541. [[CrossRef](#)]
31. Tomiki, T. Optical constants and Excton States in KCl Single Crystals. II. The Spectra of Reflectivity and Absorption Constant. *J. Phys. Soc. Jpn.* **1967**, *23*, 1280–1296. [[CrossRef](#)]
32. Eby, J.E.; Teegarden, K.J.; Dutton, D.B. Ultraviolet Absorption of Alkali Halides. *Phys. Rev.* **1959**, *116*, 1099–1105. [[CrossRef](#)]

33. Teegarden, K.; Baldini, G. Optical Absorption Spectra of the Alkali Halides at 10 K. *Phys. Rev.* **1967**, *155*, 896–907. [[CrossRef](#)]
34. Saito, H.; Saito, S.; Onaka, R.; Ikeo, B. Extreme ultraviolet absorption of alkali halides. *J. Phys. Soc. Jpn.* **1968**, *24*, 1095–1098. [[CrossRef](#)]
35. O’Connell-Bronin, A. Influence of cleavage in liquid helium on the shape of the  $n = 1$  exciton reflection band in KI and RbI crystals. *J. Phys.* **1994**, *6*, 2847. [[CrossRef](#)]
36. Kondo, S.I.; Nakamura, K. Strain Effects on the Fundamental Absorption in Alkali Iodides. *J. Phys. Soc. Jpn.* **1970**, *28*, 1381. [[CrossRef](#)]
37. Takahashi, S.; Kobayashi, M.; Misu, A. Piezoreflectivity Studies on Excitons and Band to Band Transitions in Alkali Bromides and Iodides under Uniaxial Stress. *J. Phys. Soc. Jpn.* **1990**, *59*, 4547–4553. [[CrossRef](#)]
38. Hashimoto, S.; Itoh, M. Excitonic structures of very thin RbI crystals. *J. Phys. Soc. Jpn.* **1986**, *55*, 739–741. [[CrossRef](#)]
39. Cardona, M.; Lynch, D. Optical Properties of the Rubidium and Cesium Halides in the Extreme Ultraviolet. *Phys. Rev. B* **1970**, *2*, 1117. [[CrossRef](#)]
40. Hashimoto, S.; Tomiie, N.; Itoh, M. Interference effect and dispersion in thin RbI crystals. *Solid State Commun.* **1985**, *54*, 1081–1084. [[CrossRef](#)]
41. Peimann, C.J.; Skibowski, M. Dielectric Properties of the Rubidium Halide Crystals in the Extreme Ultraviolet up to 30 eV. *Phys. Status Solidi* **1971**, *46*, 655–665. [[CrossRef](#)]
42. Roessler, D.M.; Walker, W.C. Exciton structure in the ultraviolet spectra of KI and RbI. *J. Opt. Soc. Am.* **1967**, *57*, 677–682. [[CrossRef](#)]
43. Hutchings, D.C.; Sheik-Bahae, M.; Hagan, D.J.; van Stryland, E.W. Kramers-Krönig relations in nonlinear optics. *Opt. Quantum Electron.* **1992**, *24*, 1–30. [[CrossRef](#)]
44. Kronig, R.D.L. On the theory of dispersion of X-rays. *Josa* **1926**, *12*, 547–557. [[CrossRef](#)]
45. Lucarini, V.; Saarinen, J.J.; Peiponen, K.E.; Vartiainen, E.M. *Kramers-Kronig Relations in Optical Materials Research*; Springer Science & Business Media: Berlin, Germany, 2005; Volume 110.
46. Aspnes, D.; Kelso, S.; Logan, R.; Bhat, R. Optical properties of  $\text{Al}_x\text{Ga}_{1-x}\text{As}$ . *J. Appl. Phys.* **1986**, *60*, 754–767. [[CrossRef](#)]
47. Weast, R.C.; Astle, M.J.; Beyer, W.H. *CRC Handbook of Chemistry And Physics*; CRC press: Boca Raton, FL, USA, 1988; Volume 69.
48. Michael, B. Properties of crystals and glasses. In *Handbook of Optics: Volume IV—Optical Properties of Materials, Nonlinear Optics, Quantum Optics*, 3rd ed.; The McGraw Hill Companies, Inc.: New York, NY, USA, 2010.
49. Pankove, J.I. *Optical Processes in Semiconductors*; Dover Publications Inc.: New York, NY, USA, 1975.
50. Portis, A.M. *Electromagnetic Fields: Sources and Media*, 1st ed.; John Wiley & Sons Inc.: New York, NY, USA, 1978.
51. Stern, F. Elementary theory of the optical properties of solids. *Solid State Phys.* **1963**, *15*, 299–408.
52. Taft, E.; Philipp, H. Photoelectric emission from the valence band of some alkali halides. *J. Phys. Chem. Solids* **1957**, *3*, 1–6. [[CrossRef](#)]
53. Arms, D.A.; Graber, T.J.; Macrander, A.T.; Simmons, R.O.; Schwoerer-Böhning, M.; Zhong, Y. Excitons in bulk liquid He 4. *Phys. Rev. B* **2005**, *71*, 233107. [[CrossRef](#)]
54. Beaglehole, D. Reflection Studies of Excitons in Liquid and Solid Xenon. *Phys. Rev. Lett.* **1965**, *15*, 551–553. [[CrossRef](#)]
55. Rowe, E.; Otte, R.; Pruett, C.; Steben, J. Operation and Performance of the University of Wisconsin-Physical Sciences Laboratory Electron Storage Ring. *IEEE Trans. Nucl. Sci.* **1969**, *16*, 159–164. [[CrossRef](#)]
56. Rubloff, G.; Fritzsche, H.; Gerhardt, U.; Freeouf, J. Far ultraviolet spectroscopy of solids in the range 6–36 eV using synchrotron radiation from an electron storage ring. *Rev. Sci. Instrum.* **1971**, *42*, 1507–1513. [[CrossRef](#)]
57. DeCicco, P.D. Self-Consistent Energy Bands and Cohesive Energy of Potassium Chloride. *Phys. Rev.* **1967**, *153*, 931–938. [[CrossRef](#)]
58. Kunz, A. Electronic Energy Bands for Rubidium Chloride and the Face-Centered Cubic Alkali Bromides. *Phys. Status Solidi* **1968**, *29*, 115–120. [[CrossRef](#)]
59. Bachrach, R.Z. The Optical Absorption of Lithium Iodide. *Phys. Lett. A* **1969**, *30*, 318–319. [[CrossRef](#)]

